

## RESEARCH ARTICLE

10.1029/2019JC014962

## Key Points:

- The layered circulation in SCS is formed and sustained by the coupled dynamics of external forcing through straits and internal response of vertical transport
- The vertical transport is associated with the cross-slope motion due to slope current-topography interaction and links the circulation in the different layers
- The vorticity induced by the internal vertical transport is the major response to the external vorticity flux in the middle and lower layers

## Supporting Information:

- Supporting Information S1

## Correspondence to:

J. Gan,  
magan@ust.hk

## Citation:

Cai, Z., & Gan, J. (2019). Coupled external-internal dynamics of layered circulation in the South China Sea: A modeling study. *Journal of Geophysical Research: Oceans*, *124*, 5039–5053. <https://doi.org/10.1029/2019JC014962>

Received 12 FEB 2019

Accepted 4 JUN 2019

Accepted article online 26 JUN 2019

Published online 22 JUL 2019

## Coupled External-Internal Dynamics of Layered Circulation in the South China Sea: A Modeling Study

Zhongya Cai<sup>1</sup>  and Jianping Gan<sup>1</sup> 

<sup>1</sup>Department of Mathematics and Department of Ocean Science, The Hong Kong University of Science and Technology, Hong Kong, China

**Abstract** The external inflow/outflow through straits on the periphery of the South China Sea (SCS) and the associated internal response of vertical transport over the broad continental slope form and sustain a cyclonic-anticyclonic-cyclonic (CAC) circulation in the upper-middle-lower layer in the SCS. We conduct a process-oriented numerical study to investigate the underlying coupled external-internal dynamics that remains unknown, despite that the dynamics plays a critical role in forming and sustaining the CAC circulation. External sandwich-like inflow-outflow-inflow in the water column through the Luzon Strait forms a three-dimensional CAC slope current over the curving slope topography in the SCS basin, in which the downward/upward transport associated with the cross-slope motion is established. The along-slope current over the basin provides vorticity through the beta effect and accounts for the most external planetary vorticity input through the strait in the upper layer of the SCS, while the vorticity induced by the vertical transport is the major response to the external vorticity flux in the middle and lower layers. We illustrate the critical role of the vertical transport in linking the vorticity among the different layers for the development and sustenance of the CAC circulation. The vertical transport is associated with the cross-slope motion due to slope current-topography interaction, which involves mainly in bottom frictional transport and geostrophic cross-isobath transport by the pressure gradient force in the along-slope direction. Pressure gradient force is generated by nonlinear vorticity advection and the beta effect of the background slope current.

**Plain Language Summary** The unique cyclonic-anticyclonic-cyclonic (CAC) circulation in the upper-middle-lower layer has been recognized in South China Sea (SCS) and the previous studies mainly focused on the links between the layered circulation and external forcing through the strait on the periphery of the SCS. However, the internal processes as in response to the external forcing and the role of coupled external-internal dynamics in regulating the CAC circulation have not been adequately addressed. Using process-oriented numerical simulation, this study explores the formation process of the CAC circulation and investigate the underlying coupled external-internal dynamics. Driven by the external inflow-outflow-inflow in the water column through the Luzon Strait, the three-layer CAC slope current is formed with the establishment of downward/upward transport. The vertical transport between the different layers mainly occurs over the slope because of the cross-slope motion, which is induced by the bottom friction and pressure gradient forcing in the along-slope direction. The vertical transport plays a critical role in linking the vorticity among different layers for the development and sustenance of the CAC circulation particularly in the middle and lower layers. This study improves the understanding of dynamics in the layered ocean circulation of the SCS.

### 1. Introduction

The South China Sea (SCS) is the largest marginal sea in the tropics (Figure 1). It consists of a deep basin, a shallow broad shelf in the northern and southern parts, and a steep continental slope in the eastern and western parts. It is connected to the East China Sea through the Taiwan Strait, to the Pacific Ocean through the Luzon Strait (LS), to the Sulu Sea through the Mindoro Strait (MS), and to the Java Sea through the Karimata Strait (KS).

The seasonal Asian monsoon and the Kuroshio intrusion through the LS strongly influence the circulation in the SCS (Fang et al., 2009; Gan et al., 2006; Gan, Liu, & Hui, 2016; Gan, Liu, & Liang, 2016; Qu, 2000; Qu

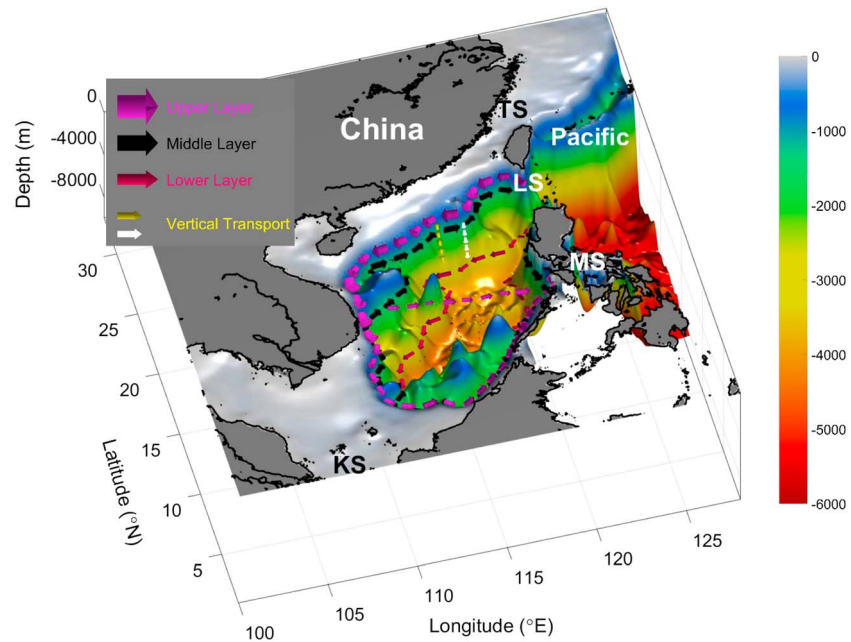


**Figure 1.** Schematic annual mean CAC circulation, based on Stokes's Theorem, in the South China Sea. Color contours represent bathymetry (m). LS: Luzon Strait; TS: Taiwan Strait; MS: Mindoro Strait; and KS: Karimata Strait.

et al., 2009; Su, 2004; Xu & Oey, 2014; Xue et al., 2004; Yuan, 2002). The winter/summer monsoon drives a southwestward/northeastward upper-layer current along the continental margin in the northern and western parts of the SCS. As a result, the basin circulation in the upper layer is cyclonic in winter, and cyclonic/anticyclonic in the northern/southern half of the basin in summer (Qu, 2000). However, for the upper layer above a depth of 750 m, the annual mean domain-averaged circulation is cyclonic (Gan, Liu, & Hui, 2016). Compared to the upper layer, we know little about the circulation in the deeper layers of the SCS. G. Wang et al. (2011) and Lan et al. (2013, 2015) used hydrographic data and numerical simulations to show the existence of cyclonic circulation in the deep layer. Gan, Liu, and Hui (2016) proposed a cyclonic-anticyclonic-cyclonic (CAC) circulation with the layers separated at the depths of 750 and 1500 m (Figure 1). They dynamically linked the CAC circulation to the exchange flows through the straits surrounding the SCS.

The SCS circulation is recognized to be driven largely by the transport through the LS, which is also the only deep channel (~2,500 m deep) connecting the SCS to the open ocean while the other straits surrounding the SCS are much shallower. When Kuroshio passes by LS, a branch of the Kuroshio flows northwestward into the SCS basin. Most of the intruding water circulates over the slope and leaves the basin mainly through the KS and MS (Gan, Liu, & Liang, 2016; Qu et al., 2006). Observations and various numerical modeling studies have revealed a sandwich-like inflow-outflow-inflow pattern in the upper-middle-lower layers of the LS, respectively (e.g., Tian et al., 2006; Xu & Oey, 2014). Annual-mean westward transports from the Pacific to the SCS through the LS have been widely reported (e.g., Chen & Huang, 1996; Qu, 2000; Tian et al., 2006; Wyrski, 1961; Xue et al., 2004), and the mean and variability of the LS transport are largely controlled by the large-scale forcing in the Pacific Ocean (e.g., Qu et al., 2005; Wang et al., 2006). The volume transports through the LS in the upper, middle, and lower layers (Gan, Liu, & Liang, 2016) were estimated to be  $-5.9$ ,  $1.4$ , and  $-0.9$  Sv, respectively. With the outward transports in the shallower Taiwan Strait, MS, and KS in the upper layer and the semienlosed (open to the LS only) deep basin, a downward mass flux from the upper layer and an upward mass flux from the lower layer must occur to compensate for the outflow in the middle layer of the LS (Liu & Gan, 2017). So far, we know little about the detailed internal response to external forcing in the CAC circulation.

Previous studies mainly focused on the role of external forcing, that is, the sandwich-like Kuroshio intrusion through the LS, in the formation of the layered basin circulation. For example, using the simplified one-layer model developed by Yang and Price (2000), the formation of the SCS deep circulation was explained based

on the potential vorticity integral constraint (Lan et al., 2013; Xu & Oey, 2014; Zhu et al., 2017). In addition, Lan et al. (2015) revealed that the deep-water overflow through the LS contributed to the seasonal variability of the SCS's deep circulation. In those studies, the physical rationale behind the circulation was derived from the simplified single-layer model, and the circulation was assumed to be independent of depth. The curl of the friction was amplified as the sole process responding to the external potential vorticity flux, which does not physically accommodate the actual multilayer CAC circulation. Using the results from a three-dimensional model, Gan, Liu, and Hui (2016) revealed that the three-layer CAC basin circulation in the SCS was induced by the planetary vorticity flux of the inflow-outflow-inflow structure in the LS extrinsically.

However, previous studies did not elaborate the response of the internal dynamics in the SCS to the external forcing. Yet, the internal and external dynamics are dynamically coupled to regulate the CAC circulation. In particular, previous studies did not investigate the vertical transports associated with the flow-topography interaction over the broad slope in the SCS. These vertical transports play a critical role in linking the vorticity among the different layers for the development and sustenance of the CAC circulation. This study investigates these important internal and coupled dynamics and fills the gaps in our understanding of the forcing mechanism of the CAC circulation in the SCS.

## 2. The Numerical Ocean Model

The ocean model used is the Regional Ocean Model System (Shchepetkin & McWilliams, 2005) for three-dimensional, time-dependent flow governed by the hydrostatic primitive equations. A local closure scheme based on the Level 2.5 turbulent kinetic energy equations developed by Mellor and Yamada (1982) is adopted in the vertical mixing parameterization.

To isolate the physics and identify the associated forcing mechanism of the layered circulation, we adopt an idealized geometry that preserves the spatial scale and characteristic of the SCS, similar to that of Cai and Gan (2017). In this process-oriented modeling study, the SCS basin model domain is represented by a circularly shaped basin (Figure 2a). Our sensitivity experiments with different basin geometries and water depths show that the formation of the CAC circulation is not qualitatively sensitive to the basin geometry in this process-oriented modeling study, as expected by the role of planetary vorticity flux in the CAC circulation (Gan, Liu, & Hui, 2016). The radius of the idealized circular basin is designed to be 800 km based on the width of the SCS. The basin's slope topography is narrower and steeper to the west just as in the real SCS, and its width gradually increases toward the southern and northern ends. The water depth increases linearly from 400 m to 2,500 m over the slope. Since the lower-layer cyclonic circulation in the SCS exists below 1,500 m (Gan, Liu, & Hui, 2016) due to the deep inflow through the LS, we use a flat bottom at a depth of 2500 m in the interior deep basin. The similar CAC circulation can be formed in the sensitivity experiment with central deep basin of depth 4,000 m.

Because most of the intruding water through the LS moves to the southern part and leaves the basin through the MS (Gan, Liu, & Liang, 2016), we adopt only two straits on the northeastern and southeastern boundaries to represent the LS and MS. In the northern SCS, the isobaths link directly to the LS and the northern slope extends horizontally into the northern strait. The depth of the southern strait is set to 400 m to represent the shallow southern passages of the MS. Our idealized basin realistically characterizes the topography of the SCS and mimics the physical conditions of the SCS so that we can identify the processes and dynamics underlying the formation of the SCS's layered circulation.

Our model uses a uniform horizontal rectangular grid with a grid size of 5 km. The stretched generalized terrain-following coordinate ( $s$ ; Song & Haidvogel, 1994) is adopted with 30 vertical layers. We initialize the model with horizontally uniform temperature ( $T$ ) and salinity ( $S$ ) profiles obtained from World Ocean Atlas annual mean data averaged in the SCS (Figure 2b). We set the buoyancy flux from the atmosphere to 0 for simplicity, which will not affect qualitatively the results of this study according to our numerical experiment. We also set the initial velocities and elevation to 0. The no-gradient condition is applied to the surface elevation along the open boundaries. Horizontal diffusion processes are represented by a harmonic viscosity with a constant eddy coefficient ( $10 \text{ m}^2/\text{s}$ ).

The layered CAC circulation in the SCS is mainly induced by external forcing through the straits (Gan, Liu, & Hui, 2016). Thus, wind forcing is neglected in this process-oriented simulation to isolate the response to

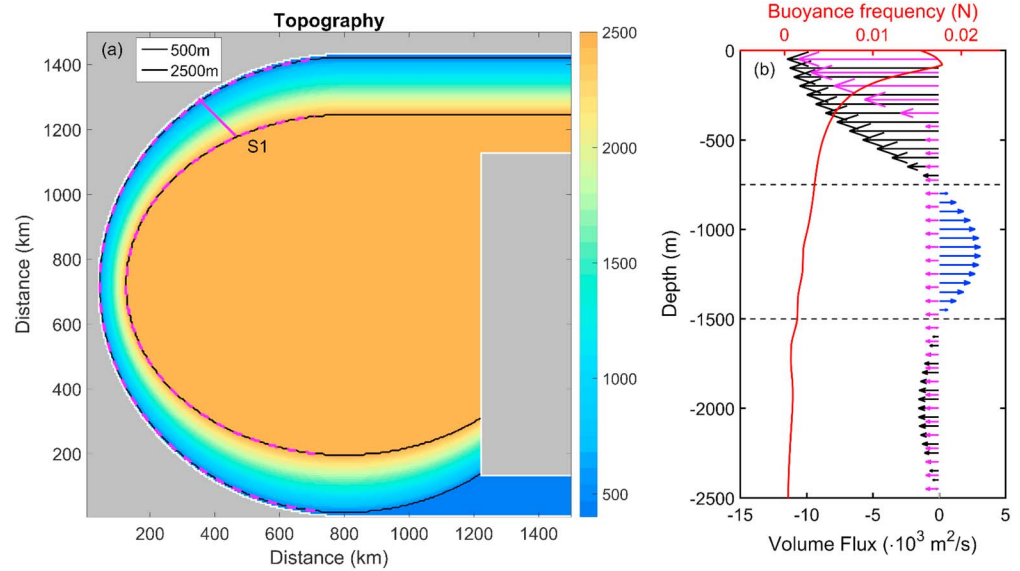


**Figure 2.** (a) Topography used in the idealized numerical study. The thin and thick black lines depict the 500- and 2,500-m isobaths. The purple dashed lines define the region of the western slope, and the purple line depicts the cross-slope transect S1. (b) Vertical profile of buoyancy frequency (red line) and volume flux ( $10^3 \text{ m}^2/\text{s}$ ) through the northern strait in Case\_s (black and blue arrows) and Case\_a (purple arrows).

the lateral boundary forcing. The mean magnitude of the westward transport through the LS ranges between 3 and 6.5 Sv (Hsin et al., 2012), and 5 Sv is adopted. In the standard case (Case\_s), the model is driven by the three-layer inflow-outflow-inflow structure in the northern strait using a trigonometric function (Figure 2b). The three layers are separated at the depths of 750 and 1,500 m, and the volume transports in the upper, middle, and lower layers are  $-5.5$ ,  $1.5$ , and  $-1$  Sv, respectively. The zonal velocity through the strait is made horizontally uniform and is calculated from the volume flux at each depth. In the southern strait, the radiation boundary condition is used. The daily-averaged model results of the first 6 months (180 days) that are established by the inflow/outflow of the external forcing to a quasi-steady state are used to isolate the formation process of the CAC circulation and underlying dynamics in this process-oriented study. The basic circulation structure and balance pattern remain the same in the sensitivity experiment of long-term run (10 years).

To explore the effects of the intrinsic flow-topography interaction over the broad slope on the formation of the layered circulation, we conduct an additional sensitivity experiment (Case\_a) where we use a different inflow structure through the northern strait. A one-layer inflow with a total transport of 5 Sv is used in Case\_a (Figure 2b), but it has a different vertical structure calculated by

$$U_{in}(z) = -\frac{Q_1}{L} \frac{2H_1}{\pi} \sin\left(\frac{\pi}{2H_1}z_1 + \frac{\pi}{2}\right) - \frac{5-Q_1}{2500L}; \quad z_1 = \min(z, H_1), \quad (1)$$

where  $H_1$  is the depth of the upper part in which the volume flux decreases vertically following a sine function,  $Q_1$  is the transport (Sv) in the upper part, and  $L$  is the width of the northern strait. In Case\_a, to identify the role of upward transport from the deep ocean, the upper inflow through the northern strait is made to occur above 400 m; that is,  $H_1 = 400$  m. Because of this constraint, the intruding water flows just above the basin slope and exits the basin through the southern strait without strong direct interaction with bottom topography. We set  $Q_1$  to 2.5 Sv, and thus, the intensity of the circulation below  $H_1$ , which is represented by  $5 - Q_1$  in equation (1), would be strong enough to influence the circulation above  $H_1$ .

### 3. Formation of the Layered Circulation

We depict the layered circulation using the domain-averaged vorticity in the water column. According to Stokes's theorem,

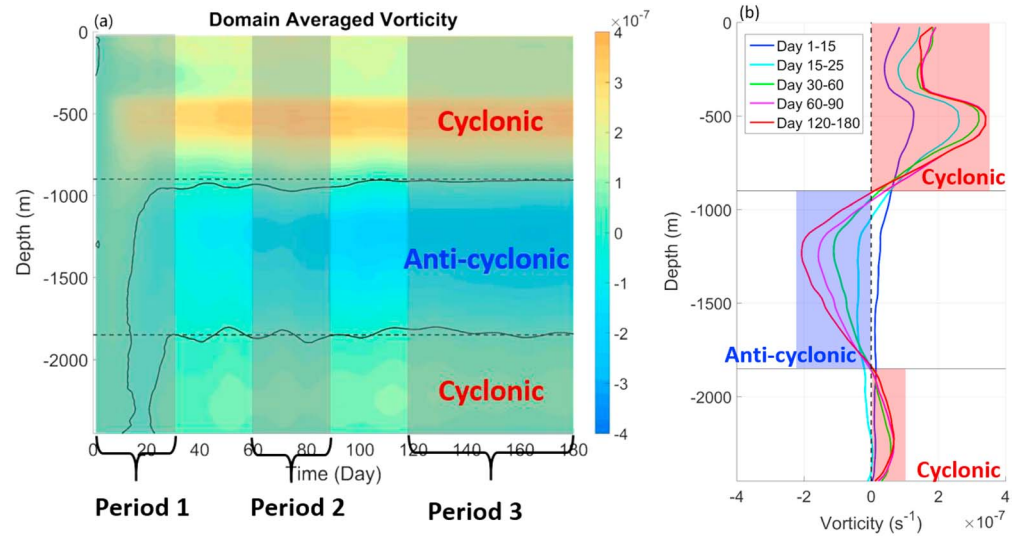


**Figure 3.** (a) Time series of domain-averaged vorticity ( $\text{s}^{-1}$ ) as a function of depth in Case\_s. The two black dashed lines indicate the depths of 900 and 1,850 m. (b) Vertical profile of domain-averaged vorticity during different periods.

$$\Gamma = \oint \vec{V} dl = \iint \zeta dA, \quad (2)$$

where  $\Gamma$  is the basin circulation,  $\vec{V}$  is the velocity vector, and  $\zeta$  is the vertical relative vorticity normal to  $A$ , the area of the inner basin. Figure 3a shows the time series of the domain-averaged vorticity as a function of depth for Case\_s. There is a clear three-layer alternating CAC circulation in the upper ( $<900$  m), middle (900 to 1,850 m), and lower ( $>1,850$  m) layers of the water column. In the early stages of the run before day 15, the circulation exhibits a single layer with positive vorticity decreasing with depth. A two-layer circulation is generated between Days 15 and 25. The averaged positive and negative vorticities above and below  $\sim 1,050$  m are  $1.3 \times 10^{-7}$  and  $-2.3 \times 10^{-8} \text{ s}^{-1}$ , respectively. After Day 25, an additional cyclonic circulation is formed below 1,850 m to produce the three-layer CAC circulation. The vorticities in the upper, middle, and lower layers between days 30 and 60 are  $1.8 \times 10^{-7}$ ,  $-6.8 \times 10^{-8}$ , and  $3.6 \times 10^{-8} \text{ s}^{-1}$ , respectively. The intensity of circulation in each layer increases gradually with time, but the basic vertical structure of the layered circulation is stable after formation. In the quasi-steady state (after day 120), the average vorticities in the upper, middle, and lower layers reach  $1.9 \times 10^{-7}$ ,  $-1.2 \times 10^{-7}$ , and  $4.5 \times 10^{-8} \text{ s}^{-1}$ , respectively.

For Case\_s, we define three distinct periods, as shown in Figure 3a, to depict different stages of the layered circulation. We will describe its temporal evolution in Period 1 (the first 30 days), Period 2 (the next 30 days), and Period 3 (the last 60 days). Because the layered circulation mainly flows along the basin slope, we show the along-isobath velocity averaged over the bottom 50 m during these three periods in Figures 4a–4c. During Period 1, the current flows cyclonically over most of the slope and an anticyclonic slope current exists only in the middle part of the northern slope. During Period 2, the intensity of the basin circulation increases in each layer, and the anticyclonic slope current in the middle layer extends from the northern part to the entire slope. The basic pattern of slope current during Period 3 is similar to that in Period 2 except with greater intensity. The horizontal basin circulations also clearly display the three-layer cyclonic, anticyclonic, and cyclonic structure (supporting information Figure S1).

During the development of the CAC circulation, the cross-isobath velocity forms over the slope (Figures 4d–4f). During Period 1, the cross-isobath velocity only has a two-layered structure, or offshore motion over the upper part of the slope and an onshore motion over the rest. It should be noted that, over the southern slope, the onshore motion exists in the region with the cyclonic slope current, although the bottom friction of the cyclonic current should induce offshore motion in Ekman balance. Similarly, over the northern slope, the nonfrictional offshore motion also occurs in some regions with the anticyclonic

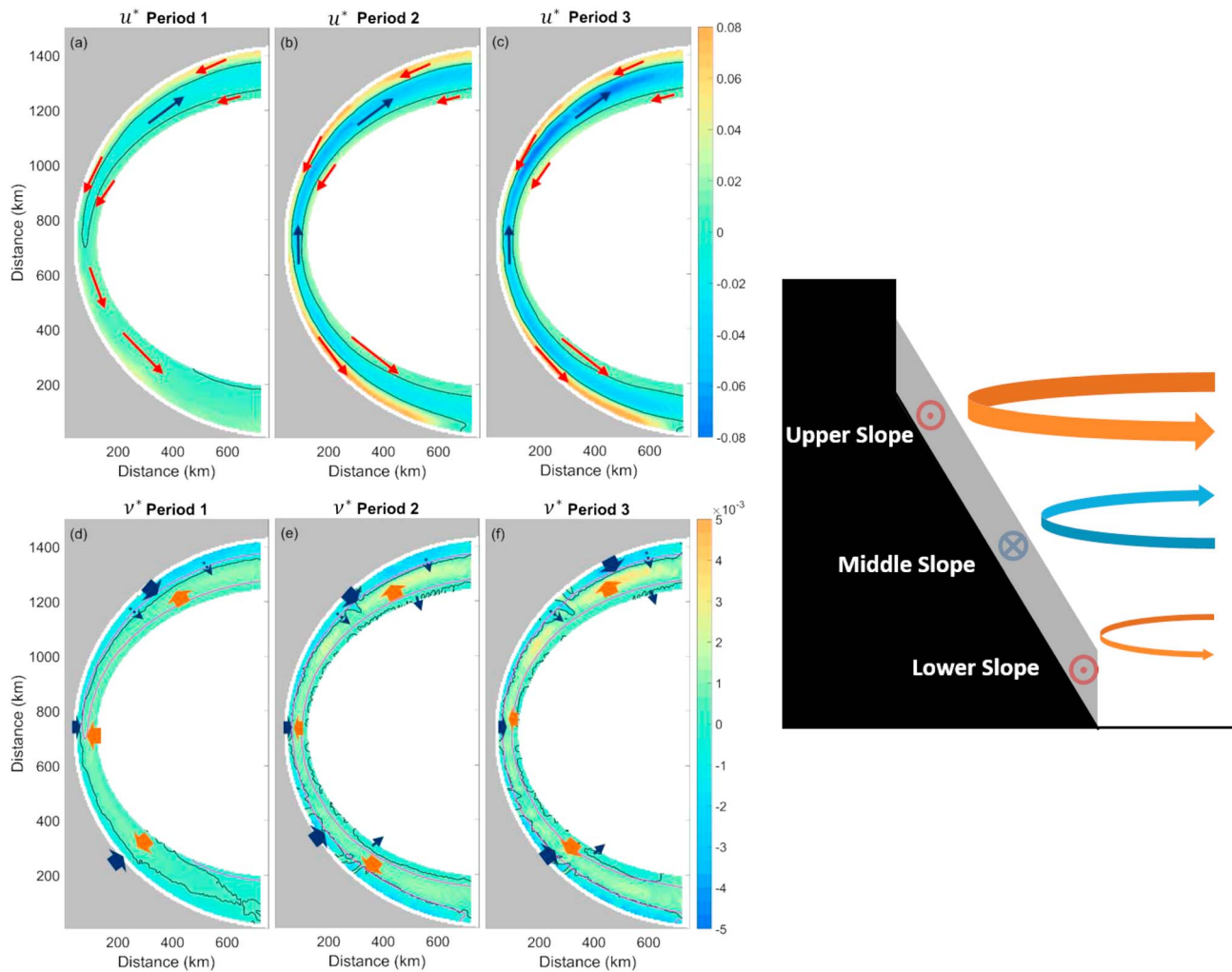


**Figure 4.** (a–c) Horizontal map of the bottom-averaged (50 m) along-isobath velocities ( $u^*$ ) in Periods 1 to 3 in Case\_s. Positive values indicate the cyclonic velocities, and black lines show the locations where the along-isobath velocity equals zero. (d–f) The same as (a)–(c) but indicate the cross-isobath velocities ( $v^*$ ). Positive values indicate the onshore velocities. Black and purple lines show the locations where the cross- and along-isobath velocities equal zero. The panel to the right illustrates the locations of the upper, middle, and lower layers of the slope.

slope current. During Period 2, the offshore motion forms over the lower slope, but its intensity is much weaker than that over the upper slope and it exists only in a small region. Over the upper and middle parts of slope, the cross-isobath velocity flows offshore and onshore, respectively. Similar to Period 1, the offshore motion occupies the upper part and extends to the middle part over the northern slope. The basic patterns of the cross-isobath velocities during Period 3 are very similar to those during Period 2. Generally, the cross-isobath velocity is correlated with the along-isobath velocity but has a different spatial distribution, which indicates that processes other than bottom friction also contribute to the cross-isobath motion. This will be discussed in section 4.2 below.

We use a cross-slope transect S1, shown in Figure 2a, as an example to illustrate the vertical structure of the layered circulation. Because the basic patterns of the slope current are similar during Periods 2 and 3, we show only the result from Period 1 when the basin circulation is forming and the result from Period 3 when the circulation becomes relatively stable (Figure 5). During Period 1, the cyclonic, anticyclonic, and cyclonic slope currents mainly occur over the upper (<1,000 m), middle (1,000 to 2,150 m), and lower (>2,150 m) parts of the slope, respectively. However, the cross-isobath velocity during Period 1 only has two layers with offshore (downward) motions above 1,200 m and onshore (upward) motions below 1,200 m of the slope (Figure 5c). During Period 3, the intensity and the detail structure of slope current vary with the internal baroclinic adjustment but the basic layered circulation pattern of the along-isobath velocity is similar to that

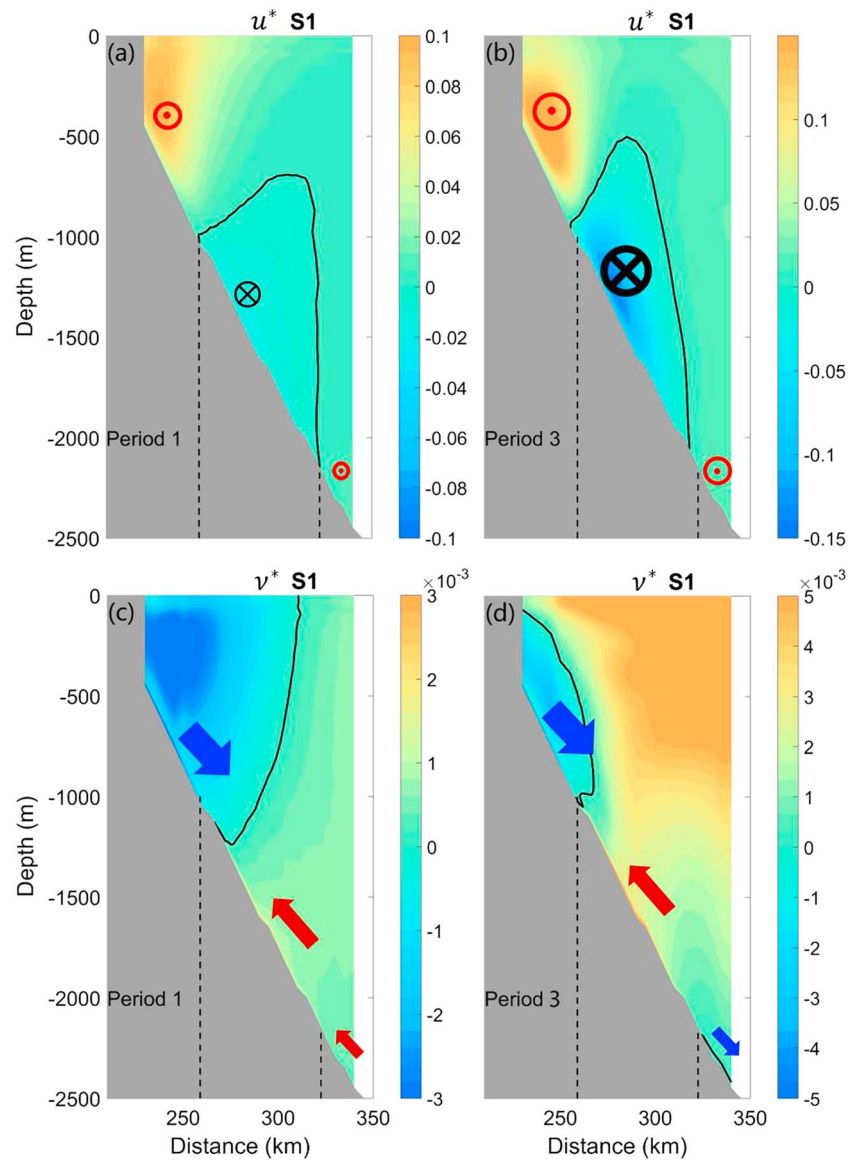


**Figure 5.** (a, b) Vertical profiles of the along-isobath velocity ( $u^*$ , m/s) at transect S1 during Period 1 and Period 3 for Case\_s. A positive value indicates a cyclonic velocity. (c, d) The same as (a) and (b) but indicate the cross-isobath velocities ( $v^*$ , m/s), and a positive value indicates an onshore velocity. The black dashed lines indicate the depths of 1,000 and 2,150 m.

during Period 1. For the cross-isobath motion, the offshore (downward) motion exists above 1,000 m and also over the lower slope, but the lower slope offshore motion is much weaker and confined to a very thin layer near the bottom (Figures 5b and 5d).

Considering the shallower southern strait and the inflow-outflow-inflow structure through the northern strait, vertical mass fluxes from the upper and lower layers might exist to compensate for the outflow in the middle layer. The vertical transport could be largely associated with the cross-isobath motions over the basin slope as shown in Figures 4 and 5. To further confirm this, we calculate the divergence/convergence of the water in the upper layer (<900 m) and lower layer (>1,850 m) over the slope region and compare the results with the outflux of water through the northern strait in the middle layer (900 to 1,850 m). Figure 6 shows that, except during the very beginning of the run, the vertical transports over the slope from the upper and lower layers account for most of the middle layer's outflow.

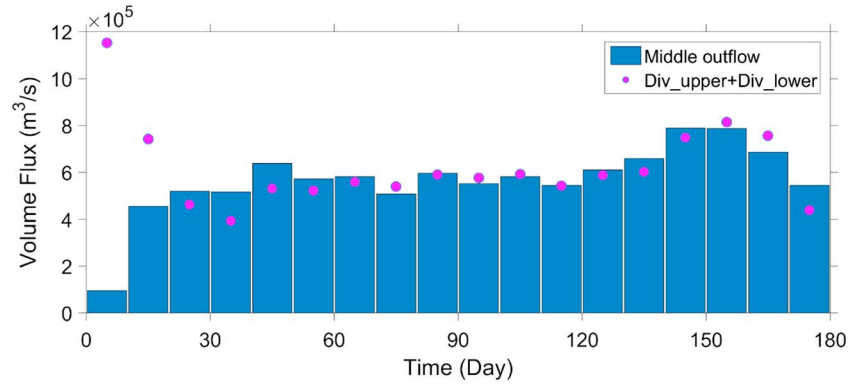


**Figure 6.** A 10-day-averaged middle layer outflow through the northern strait (blue bars) and the sum of the water divergence in the upper and lower layers over the slope (purple circles) for Case\_s.

## 4. Discussion

### 4.1. Vorticity Dynamics

To identify the dynamics governing the formation of the layered circulation in the basin, the domain-integrated vorticity balance (Gan, Liu, & Hui, 2016) in each of the layers is used:

$$\begin{aligned}
 \underbrace{\int_A \left[ \nabla \times \int_{L_b}^{L_u} \vec{V}_t dz \right] dA}_{\text{VOR\_ACCE}} &= \underbrace{-\int_A \left[ \nabla \times \int_{L_b}^{L_u} \text{HNL} dz \right] dA}_{\text{VOR\_ADV}} - \underbrace{\int_A \left[ \nabla \times \int_{L_b}^{L_u} \text{VNL} dz \right] dA}_{\text{VOR\_PGF}} + \int_A \left[ \nabla \times \int_{L_b}^{L_u} \text{PGF} dz \right] dA \quad (3) \\
 \underbrace{-\int_A \left[ f \nabla \cdot \int_{L_b}^{L_u} \vec{V} dz \right] dA}_{\text{VOR\_DIV}} - \underbrace{\int_A \left[ \beta \int_{L_b}^{L_u} v dz \right] dA}_{\text{VOR\_COR}} &+ \underbrace{\int_A \left[ \nabla \times \int_{L_b}^{L_u} \text{VVIS} dz \right] dA}_{\text{VOR\_VVIS}} + \underbrace{\int_A \left[ \nabla \times \int_{L_b}^{L_u} \text{HVIS} dz \right] dA}_{\text{VOR\_HVIS}},
 \end{aligned}$$

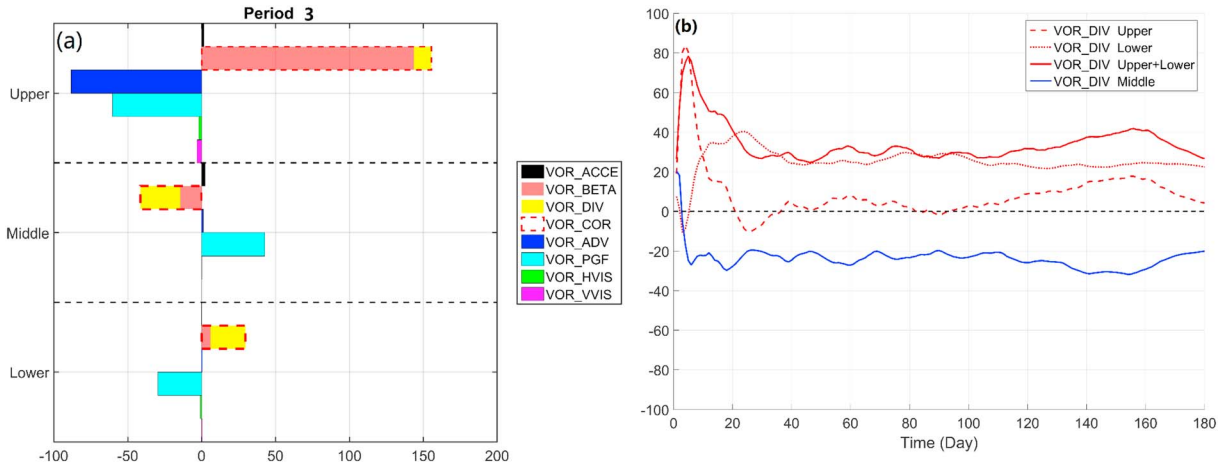
where the terms  $L_u$  and  $L_b$  are the depths of the top and bottom of each of the three layers and are defined as (0 and 900 m), (900 and 1,850 m), and (1,850 and 2,500 m).  $A$  is the domain of the basin;  $u$  and  $v$  are the velocities in the zonal ( $x$ ) and meridional ( $y$ ) directions;  $f$  is the Coriolis parameter, and  $\beta$  is the meridional gradient of  $f$ .  $HNL$  and  $VNL$  are the horizontal and vertical nonlinear advection terms.  $HVIS$  and  $VVIS$  are the horizontal and vertical viscous terms.

Figure 7a shows that in the upper layer, the term  $\text{VOR\_COR}$  provides the positive vorticity, which, after applying the divergence theorem (Gauss-Ostrogradsky theorem), represents the net planetary vorticity flux through the two straits (Gan, Liu, & Hui, 2016). The intruding planetary vorticity can be divided into two terms,  $\text{VOR\_BETA}$  and  $\text{VOR\_DIV}$ , which represent the vorticity formation due to the horizontal and vertical motions of the water.

The input of planetary vorticity from LS in the northern basin contributes mainly to the beta effect ( $\text{VOR\_BETA}$ ) rather than to the divergence effect ( $\text{VOR\_DIV}$ ) in the upper layer. This is because that the intruded waters from LS exit the basin mainly from other southern straits in the upper layer, while a stronger meridional velocity also leads to a larger beta effect in the layer. The magnitudes of  $\text{VOR\_DIV}$  in the semi-closed middle and lower layers are thus relatively large.

At the same time, the positive  $\text{VOR\_DIV}$  indicates downward transport from the upper layer to the middle layer as shown in Figure 5. The major responses to the vorticity influx through the LS are  $\text{VOR\_PGF}$  and  $\text{VOR\_ADV}$ .  $\text{VOR\_PGF}$ , or the bottom pressure torque, is formed due to the interaction between pressure gradient and the variable slope topography (Mertz & Wright, 1992).

In the semienclosed (open only to the northern strait) middle layer, the outflow through the LS induces a negative  $\text{VOR\_COR}$ , which is balanced by the positive  $\text{VOR\_PGF}$ . The middle layer differs from the



**Figure 7.** Terms ( $\text{m}^3/\text{s}^2$ ) in equation (3) in the upper, middle, and lower layers during Period 3 for Case\_s. (b) Time series of VOR\_DIV averaged over the respective upper, middle, and lower layers for Case\_s.

upper layer in that VOR\_DIV is larger than VOR\_BETA, which means the vorticity outflux through the northern strait is mainly provided by the vertical transport of water instead of the horizontal motion. In the lower layer, the vorticity balance is similar to the balance in the middle layer, but with opposite signs.

The time series of VOR\_DIV in the different layers (Figure 7b) shows that VOR\_DIV in the upper and lower layers vary similarly, but with an opposite sign to VOR\_DIV in the middle layer, except very early on. This suggests that the vertical transports from the upper and lower layers produce negative VOR\_DIV in the middle layer. G. Wang et al. (2012) similarly revealed that the anticyclonic circulation component (negative vorticity) was induced in a layer by upwelling from the base of the layer. Therefore, the vorticity input induced by the vertical transport of water is the major response to the external vorticity flux in the middle and lower layers and can act as an intrinsic link between the circulations in different layers.

#### 4.2. Along-Isobath Momentum Dynamics

The layered circulation is formed mainly by the basin-circular flows along the slope as shown in Figure 5. Furthermore, the vertical transports associated with the cross-isobath motions over the slope provide most of the middle-layer outflow through the northern strait (Figure 6). Therefore, we focus on the cross-isobath motion over the slope.

We investigate the underlying dynamics using the along-isobath momentum balance. To link it with the depth-integrated vorticity dynamics as discussed below, the along-isobath momentum balance is multiplied by the slope of bottom topography:

$$v_t^* \cdot H_x^* = \underbrace{-ADV \cdot H_x^*}_{\text{Along\_ADV}} - \underbrace{fu^* \cdot H_x^*}_{\text{Along\_COR}} - \underbrace{\frac{1}{\rho} P_{y^*} \cdot H_x^*}_{\text{Along\_PGF}} + \underbrace{HVVIS \cdot H_x^*}_{\text{Along\_HVVIS}} + \underbrace{VVVIS \cdot H_x^*}_{\text{Along\_VVIS}} \quad (4)$$

where  $v_t^*$  refers to the along-isobath acceleration. The terms on the right-hand side are the nonlinear advection (ADV), which includes horizontal and vertical advection; Coriolis force (COR); pressure gradient force (PGF); horizontal viscosity (HVVIS); and vertical viscosity (VVVIS).  $H_x^*$  is the slope of the bottom topography. The subscripts  $x^*$  and  $y^*$  represent partial differentiation in the cross-isobath and along-isobath directions, respectively;  $x^*$  is positive in offshore direction, and  $H_x^*$  has positive value;  $y^*$  is positive in the anticyclonic direction along the isobath so that a positive/negative Along\_COR indicates onshore/offshore motion.

Figure 8 shows the vertical structure of the major terms in equation (4) during Period 3. The Along\_COR has the same structure as the cross-isobath velocity over the slope. The effect of friction (Along\_VVIS) exists mainly near the bottom and contributes to the cross-isobath motion especially over the upper (<950 m) and middle (950 to 2,100 m) parts of the slope. Away from the bottom friction layer, the cross-isobath

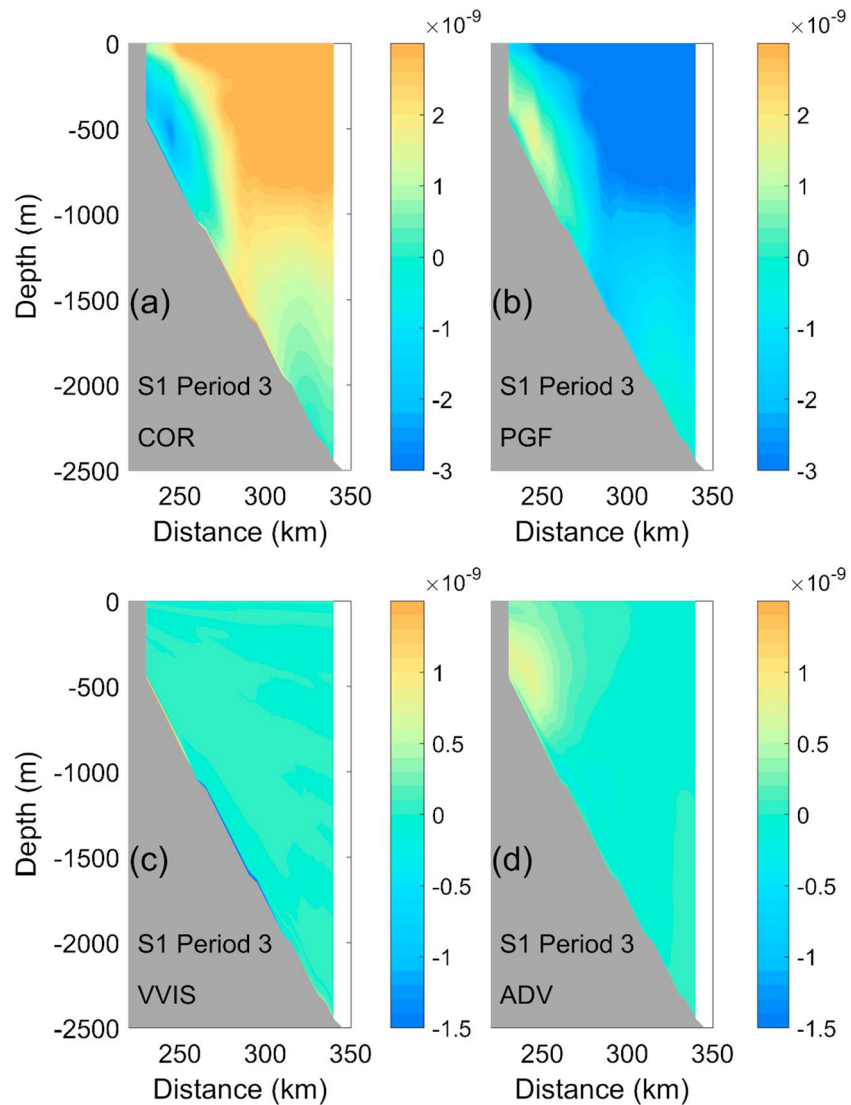


**Figure 8.** Vertical structure of major terms ( $\text{m/s}^2$ ) in equation (4) along transect S1 during Period 3 for Case\_s. COR = Coriolis force; PGF = pressure gradient force; VVIS = vertical viscosity; ADV = nonlinear advection.

motions are controlled by the geostrophic balance. Besides  $\text{Along\_VVIS}$  and  $\text{Along\_PGF}$ , the nonlinear advection  $\text{Along\_ADV}$ , which represents the spatial acceleration of the slope current over curving isobaths (Liu & Gan, 2014), also contributes to the cross-isobath motions mainly over the upper part of the slope. The magnitudes of  $\text{Along\_PGF}$  and  $\text{Along\_ADV}$  vary vertically, but their basic patterns generally remain the same from the bottom of the slope to hundreds of meters above.

The along-isobath momentum balance integrated over the bottom 50 m (Figure 9) shows the dominant effect near the bottom and geostrophic balance away from it. It can be shown that the effect of the dynamics in the bottom affect the layered circulation in the water column through vertical vorticity flux. At S1, the frictional effects ( $\text{Along\_VVIS}$ ) induced by the three-layer circulation have distinct positive, negative, and positive features over the upper (<950 m), middle (950 to 2,100 m), and lower (>2,100 m) parts of the slope, respectively (Figure 9a). Over the upper slope, the offshore motion is provided by the effects of  $\text{Along\_VVIS}$  and  $\text{Along\_ADV}$ , while the negative  $\text{Along\_PGF}$  provides the onshore motion.  $\text{Along\_PGF}$  is positive near the interface between the upper and middle parts, and it intensifies the offshore motion from the upper layer. Therefore, the offshore motion from the upper layer can extend to regions with anticyclonic circulation (Figures 4 and 5). The Ekman balance dominates the onshore motion in the middle part of S1. In

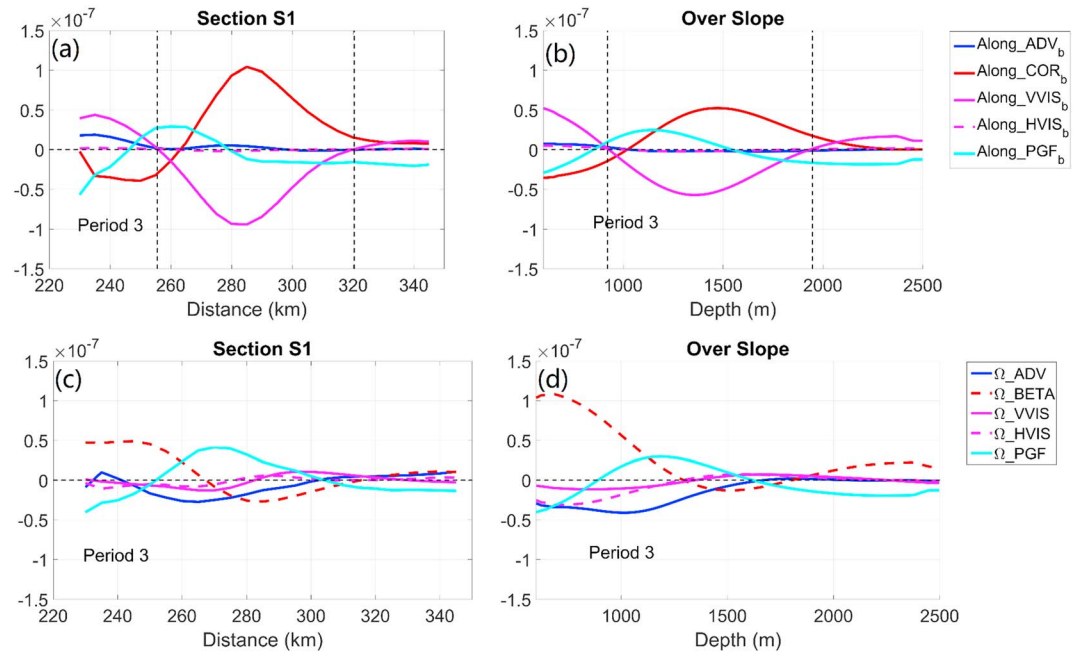


**Figure 9.** Terms ( $m^2/s^2$ ) in equation (4) integrated over the bottom 50 m (a) along transect S1 and (b) averaged along the strip (Figure 2) over the slope as a function of depth for Case\_s during Period 3. The black dashed lines indicate the locations where  $\text{Along\_VVIS}$  equals zero. (c, d) The same as (a) and (b) but for the terms ( $m/s^2$ ) in equation (5). The terms in (c) and (d) have been multiplied by 50 for comparison with the terms in (a) and (b).

the deep lower part of S1, a negative  $\text{Along\_PGF}$  provides relatively weak onshore motion. The cross-isobath motion over the entire slope (Figure 9b) exhibits a similar pattern to that along S1. The offshore/onshore motion in the upper (<950 m)/middle (950–1,950 m) part of slope is mainly provided by the bottom friction, and the onshore motion from the lower part (>1,950 m) is controlled by  $\text{Along\_PGF}$ . Near the interface between the upper and middle parts of slope, the positive  $\text{Along\_PGF}$  enhances the offshore motion from the upper part.

As shown above, the along-isobath bottom friction and PGF because of interaction between slope current and topography are the major contributors to the cross-isobath motions over the slope. The bottom friction is directly induced by the background basin circulation, while the origin of the along-isobath PGF is not clear, but it can be deduced from the depth-integrated vorticity dynamics (Gan et al., 2013):

$$\underbrace{\nabla \times \int_{-H}^0 (\text{PGF}) dz}_{\Omega\_PGF} + \underbrace{\nabla \times \int_{-H}^0 -(\text{HNL} + \text{VNL}) dz}_{\Omega\_ADV} - \underbrace{\beta \int_{-H}^0 v dz}_{\Omega\_BETA} + \underbrace{\nabla \times \left( \frac{\vec{\tau}_s}{\rho_0} - \frac{\vec{\tau}_b}{\rho_0} \text{Bigg} \right)}_{\Omega\_VVIS} + \underbrace{\nabla \times \int_{-H}^0 \text{HVIS} dz}_{\Omega\_HVIS} = 0 \quad (5)$$

The term  $\Omega\_PGF$  can be written as  $\nabla \times \int_{-H}^0 \text{PGF} dz = H_x \cdot \text{PGF}_y^b - H_y \cdot \text{PGF}_x^b = \text{PGF}_y^b \cdot H_x$ , which is mathematically equivalent to the term  $\text{Along\_PGF}$  in equation (4) at the bottom. Figures 9c and 9d show the balance of the terms from equation (5).

Generally, the formation mechanism of the along-isobath PGF over the entire slope is similar to that along S1. The beta effect ( $\Omega\_BETA$ ) of the upper- and lower-layer cyclonic slope current generates a negative along-isobath PGF. The nonlinear advection ( $\Omega\_ADV$ ) mainly produces a positive along-isobath PGF that intensifies the offshore motion from the upper layer. The contributions of other processes are relatively small. Unlike the shelf circulation with smaller spatial scale as in Gan et al. (2013), the contribution of beta effect is unneglectable. Therefore, the formation of the along-isobath PGF is largely related to the background basin circulation over the slope because of flow-topography interaction, which subsequently contributes to the cross-isobath motions over the slope for the exchange among the layers.

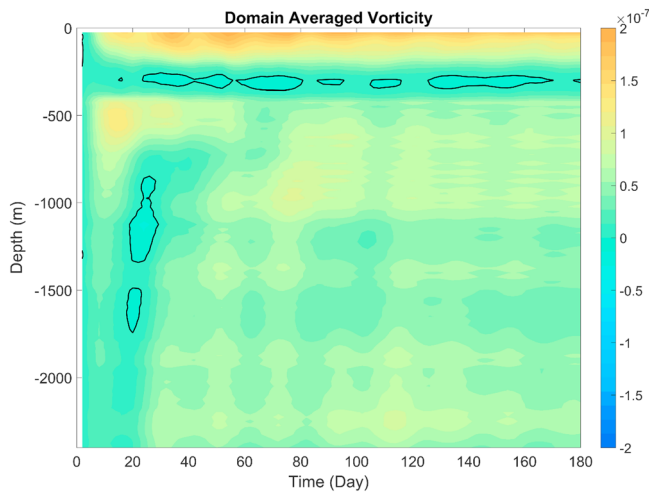


**Figure 10.** Time series of domain-averaged vorticity ( $s^{-1}$ ) as a function of depth for Case\_a. The black lines indicate the location where the vorticity is equal to 0.

### 4.3. The Role of the Lower-Layer Circulation

As indicated by the domain-integrated vorticity and along-isobath momentum dynamics, the cross-isobath motion and the associated vertical transport over the slope act as intrinsic links among the circulations in the different layers. To illustrate further the role of intrinsic processes over the slope itself, a sensitivity experiment, Case\_a, is conducted to demonstrate the formation of layered circulation through intrinsic cross-isobath motion associated with flow-topography interaction (Figure 2b).

The time series of the domain-averaged vorticity as a function of depth in Figure 10 reveals an anticyclonic circulation between  $\sim 200$  and  $400$  m embedded within a mainly cyclonic circulation in the water column. We use the evolution of the along- and cross-isobath velocities along transect S1 during Periods 1 and 3 to illustrate the formation of the layered circulation (Figure 11). Since the domain-averaged vorticity shows temporal oscillation with a negative value in the deep ocean ( $\sim 800$ – $1,800$  m) before Day 30, Periods 1 and 3 are defined as the first and last 60 days in Case\_a. During Period 1, the along-isobath velocity is cyclonic over the entire slope. Later in Period 3, it becomes an anticyclonic flow over the upper part of the slope ( $<1,000$  m). The cross-isobath motion has a two-layer

structure of offshore/onshore motion over the slope during Period 1. However, during Period 3, the offshore motion in the upper part is greatly reduced and the onshore motion almost dominates the entire slope region. The generation of the anticyclonic slope current or the formation of the layered circulation is associated with the onshore motion from the lower layer.

Like Case\_s, the deep inflow through the northern strait below  $400$  m should move upward in the semienclosed deep basin. Thus, the volume of outflow through the southern strait should be larger than the volume of inflow in the northern strait in the water column above  $400$  m. The anticyclonic circulation in the layer between  $200$  and  $400$  m (Figure 10) coincides with the net negative volume flux (Figure 12a) and the net negative vorticity flux (Figure 12b). This clearly indicates that the upward transport below  $400$  m provides negative vorticity to the layer between  $200$  and  $400$  m, as also shown in Figure 7b for Case\_s. The conditions during Periods 1 and 3 are similar, except that a stronger upward transport during Period 3 strengthens the negative vorticity in the layer between  $200$  and  $400$  m.

Horizontal distribution of Along\_COR shows that the onshore motion occurs mainly over the northern slope (supporting information Figure S2); thus, we examine the along-isobath balance that averages over the

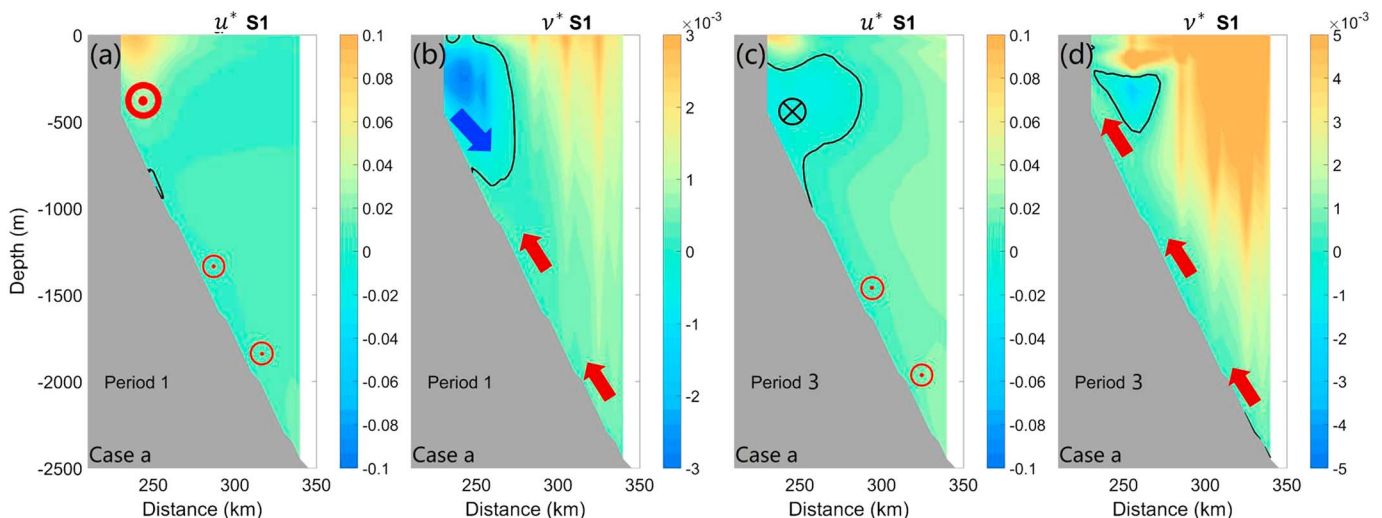


**Figure 11.** Vertical profiles of (a, c) along-isobath ( $u^*$ ) and (b, d) cross-isobath ( $v^*$ ) velocities (m/s) at S1 for Case\_a during Period 1 and Period 3.

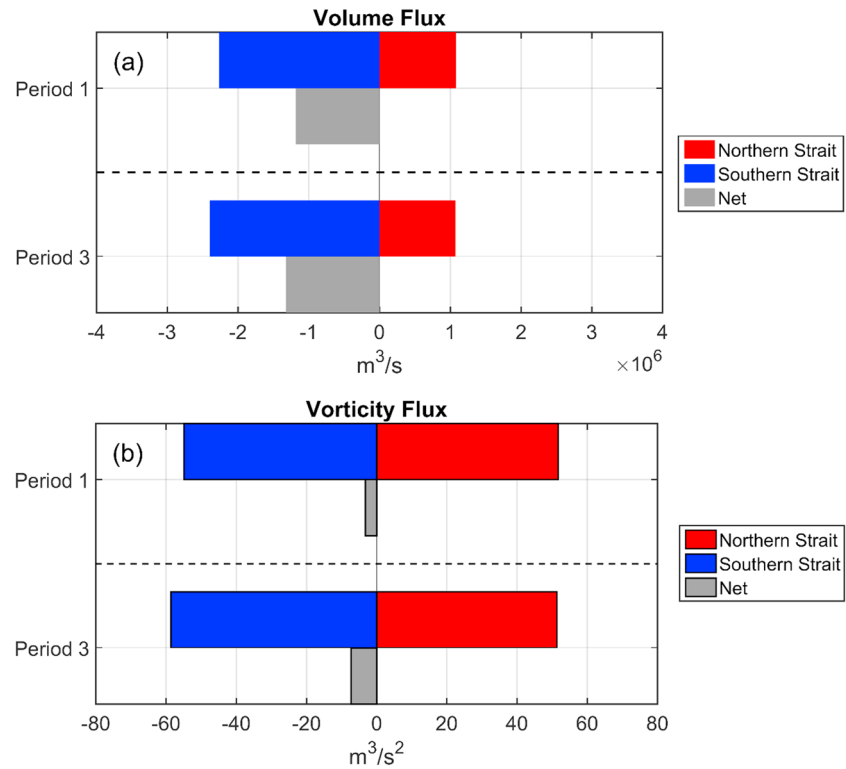


**Figure 12.** (a) Volume flux ( $m^3/s$ ) and (b) planetary vorticity flux ( $m^3/s^2$ ) in the layer between 200 and 400 m through the northern strait, southern strait, and their net flux during Period 1 and Period 3 for Case\_a. A positive value indicates an influx.

northern half of slope for Case\_a (Figure 13). Generally, the along-isobath PGF dominates the onshore motion. In this case, the upper-layer cyclonic circulation mainly flows above 400 m thus does not generate very strong bottom friction over the northern slope. The bottom friction and the nonlinear advection have negative effects, but play a smaller role compared to PGF. Like Case\_s, the negative along-isobath PGF is mainly generated by the beta effect of the inflow-driven background cyclonic circulation ( $\Omega - \text{BETA}$ ).

In general, the one-layer inflow through the northern strait in Case\_a demonstrates that a cyclonic circulation induced by the inflow can itself produce a negative along-isobath PGF through the intrinsic flow-slope interaction. This along-isobath PGF, in turn, forms an upward transport over the slope and provides negative vorticity for the formation of anticyclonic circulation in the layer between 200 and 400 m. In other words, the intrinsic process associated with flow-slope interaction redistributes the intruding vorticity and leads to the formation of a layered circulation.

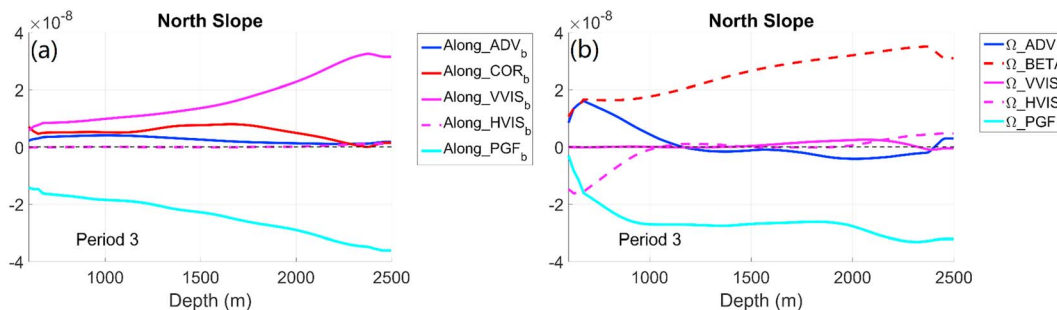


**Figure 13.** (a) Terms ( $m^2/s^2$ ) in equation (4) integrated over the bottom 50 m along the strip (Figure 2) over the northern half of the slope as a function of depth for Case\_a during Period 3. (b) The same as (a) but for the terms ( $m/s^2$ ) in equation (5). The terms in (b) have been multiplied by 50 for comparison with the terms in (a).

## 5. Summary

The internal dynamics of the CAC circulation in the SCS are dynamically coupled with the external forcing of influx/outflux through the straits on the periphery of the SCS basin. While the formation physics of the layered circulation in the SCS in response to the coupled external-internal dynamics remains unclear. Using three-dimensional process-oriented modeling, we explored the formation process of the layered circulation and investigated underlying coupled external-internal dynamics, which is crucial to setting-up the basin circulation along the continental margin.

Driven by a sandwich-like inflow-outflow-inflow structure through the northern strait in the basin, the three-layer CAC circulation can be formed within about 1 month. The cyclonic slope current forms in the upper and lower layers, and the anticyclonic slope current exists in the middle layer. The layered structure is fairly stable once formed. While the layered circulation is developing, the cross-slope velocity and the associated vertical transport develop over the slope, creating an offshore motion over the upper part and an onshore motion over the middle and lower parts of slope. The offshore motion also occurs over the lower part of the slope, but its magnitude is strongly reduced and the motion is confined to a small region.

The formation process of the CAC circulation is largely linked to the time-dependent, three-dimensional variations of the inflow-outflow-inflow from the northern strait over the curving slope topography in the SCS basin. The underlying dynamics during the formation of the layered circulation in the SCS are illustrated by the analyses of depth- and domain-integrated vorticity for each layer.

The inflow/outflow from the northern strait drives the basin circulation by providing positive/negative planetary vorticity, which is balanced by the bottom pressure torque and nonlinear advection. After entering the basin, the intruding planetary vorticity is transported by the horizontal and vertical motions over the slope. Horizontal motions provide vorticity through the beta effect and accounts for the most planetary vorticity input through the northern strait in the upper layer, while the vorticity induced by vertical transport is the major response to the external vorticity flux in the middle and lower layers. The vertical transport links the circulation in the three layers and acts as the source/sink of vorticity, particularly in forming and sustaining the middle- and lower-layer circulation.

The vertical transport between the different layers mainly occurs over the slope because of the cross-slope motion due to flow-slope interaction including mainly the along-isobath bottom friction and PGF. Over the upper part of the slope, the along-isobath bottom friction and PGF mainly provide the offshore motion of water. The magnitude of the along-isobath PGF is small compared to the magnitude of the bottom friction, but it intensifies the downward transport near the interface between the upper and middle layers. Over the lower part of the slope, the along-isobath geostrophic balance mainly forms the onshore motion, and the bottom friction has a negative effect. The along-isobath PGF is generated by the nonlinear vorticity advection and the beta effect of the slope current and is largely linked to the background basin circulation over the slope because of flow-topography interaction. PGF subsequently contributes to the cross-isobath motion over the slope and facilitates the exchange among the different layers to aid the formation of the CAC circulation.

The coupled dynamics of the intrinsic process over the slope and external forcing through the straits determine the formation and sustenance of the CAC circulation in the SCS. The sensitivity experiment demonstrated that the intrinsic processes of the flow-topography interaction and the associated cross-isobath/vertical transport are capable of redistributing the intruding vorticity, thus leading to the formation of the layered circulation. This study explored the coupled external-internal dynamics during the formation of layer circulation in SCS in response to the lateral boundary forcing. However, the wind forcing, which is excluded in this process-oriented study, can also change the upper layer circulation and affect the vertical coupling among three layers, particularly during winter (Gan, Liu, & Hui, 2016.). Besides, during the evolution of the basin circulation, the baroclinic adjustment modulates the intensity and structure of the slope current, influences the vertical coupling among different layers, and affects the inflow/outflow pattern through the surrounding straits. The combined effect of the surface wind and lateral forcing, internal adjustment processes, and the coupled circulation between the SCS and open ocean deserve further investigation to upgrade the understanding on SCS layer circulation.

## Acknowledgments

This research was supported by the National (China) Key Basic Research Development Program (2015CB954004), and the Hong Kong Research Grants Council (GRF16204915 and GRF16206516). We are grateful for the useful comments and suggestions provided by two anonymous reviewers. The data for this study are generated from publicly distributed Regional Ocean Model System (ROMS; <https://www.myroms.org/>) and are available from the corresponding author who can be reached at [magan@ust.hk](mailto:magan@ust.hk).

## References

- Cai, Z. Y., & Gan, J. (2017). Formation and dynamics of a long-lived eddy-train in the South China Sea: A modeling study. *Journal of Physical Oceanography*, *47*(11), 2793–2810. <https://doi.org/10.1175/JPO-D-17-0002.1>
- Chen, C.-T. A., & Huang, M.-H. (1996). A mid-depth front separating the South China Sea water and the Philippine sea water. *Journal of Geophysical Research*, *101*, 17–25. <https://doi.org/10.1007/bf02236530>
- Fang, G., Wang, Y., Wei, Z., Fang, Y., Qiao, F., & Hu, X. (2009). Inter-ocean circulation and heat and freshwater budgets of the South China Sea based on a numerical model. *Dynamics of Atmospheres and Oceans*, *47*(1–3), 55–72. <https://doi.org/10.1016/j.dynatmoce.2008.09.003>
- Gan, J., Li, H., Curchitser, E., & Haidvogel, D. (2006). Modeling South China Sea circulation: Response to seasonal forcing regimes. *Journal of Geophysical Research*, *111*, C06034. <https://doi.org/10.1029/2005JC003298>
- Gan, J., Liu, Z., & Hui, C. R. (2016). A three-layer alternating spinning circulation in the South China Sea. *Journal of Physical Oceanography*, *46*(8), 2309–2315. <https://doi.org/10.1175/jpo-d-16-0044.1>
- Gan, J., Liu, Z., & Liang, L. (2016). Numerical modeling of intrinsically and extrinsically forced seasonal circulation in the China Seas: A kinematic study. *Journal of Geophysical Research: Oceans*, *121*, 4697–4715. <https://doi.org/10.1002/2016JC011800>
- Gan, J., San Ho, H., & Liang, L. (2013). Dynamics of intensified downwelling circulation over a widened shelf in the Northeastern South China Sea. *Journal of Physical Oceanography*, *43*(1), 80–94. <https://doi.org/10.1175/JPO-D-12-02.1>
- Hsin, Y. C., Wu, C. R., & Chao, S. Y. (2012). An updated examination of the Luzon Strait transport. *Journal of Geophysical Research*, *117*, C03002. <https://doi.org/10.1029/2011JC007714>
- Lan, J., Wang, Y., Cui, F., & Zhang, N. (2015). Seasonal variation in the South China Sea deep circulation. *Journal of Geophysical Research: Oceans*, *120*, 1682–1690. <https://doi.org/10.1002/2014JC010413>
- Lan, J., Zhang, N., & Wang, Y. (2013). On the dynamics of the South China Sea deep circulation. *Journal of Geophysical Research: Oceans*, *118*, 1206–1210. <https://doi.org/10.1002/jgrc.20104>
- Liu, Z., & Gan, J. (2014). Modeling study of variable upwelling circulation in the East China Sea: Response to a Coastal Promontory. *Journal of Physical Oceanography*, *44*, 1078–1094. <https://doi.org/10.1175/JPO-D-13-0170.1>
- Liu, Z., & Gan, J. (2017). Three-dimensional pathways of water masses in the South China Sea: A modeling study. *Journal of Geophysical Research: Oceans*, *122*, 6039–6054. <https://doi.org/10.1002/2016JC012511>
- Mellor, G. L., & Yamada, T. (1982). Development of a turbulence closure model for geophysical fluid problems. *Reviews of Geophysics*, *20*(4), 851–875. <https://doi.org/10.1029/RG020i004p00851>
- Mertz, G., & Wright, D. G. (1992). Interpretations of the JEBAR term. *Journal of Physical Oceanography*, *22*(3), 301–305. [https://doi.org/10.1175/1520-0485\(1992\)022<0301:IOTJT.2.0.CO;2](https://doi.org/10.1175/1520-0485(1992)022<0301:IOTJT.2.0.CO;2)
- Qu, T. (2000). Upper-layer circulation in the South China Sea. *Journal of Physical Oceanography*, *30*(6), 1450–1460. [https://doi.org/10.1175/1520-0485\(2000\)030<1450:ULCITS>2.0.CO;2](https://doi.org/10.1175/1520-0485(2000)030<1450:ULCITS>2.0.CO;2)
- Qu, T., Du, Y., Meyers, G., Ishida, A., & Wang, D. (2005). Connecting the tropical Pacific with Indian Ocean through South China Sea. *Geophysical Research Letters*, *32*, L24609. <https://doi.org/10.1029/2005GL024698>
- Qu, T., Du, Y., & Sasaki, H. (2006). South China Sea throughflow: A heat and freshwater conveyor. *Geophysical Research Letters*, *33*, L23617. <https://doi.org/10.1029/2006GL028350>
- Qu, T., Song, Y. T., & Yamagata, T. (2009). An introduction to the South China Sea throughflow: Its dynamics, variability, and application for climate. *Dynamics of Atmospheres and Oceans*, *47*(1–3), 3–14. <https://doi.org/10.1016/j.dynatmoce.2008.05.001>
- Shchepetkin, A. F., & McWilliams, J. C. (2005). The Regional Ocean Modeling System: A split-explicit, free-surface, topography following coordinates ocean model. *Ocean Modelling*, *9*(4), 347–404. <https://doi.org/10.1016/j.ocemod.2004.08.002>
- Song, Y., & Haidvogel, D. (1994). A semi-implicit ocean circulation model using a generalized topography-following coordinate system. *Journal of Computational Physics*, *115*(1), 228–244. <https://doi.org/10.1006/jcph.1994.1189>
- Su, J. L. (2004). Overview of the South China Sea circulation and its influence on the coastal physical oceanography outside the Pearl River Estuary. *Continental Shelf Research*, *24*(16), 1745–1760. <https://doi.org/10.1016/j.csr.2004.06.005>
- Tian, J., Yang, Q., Liang, X., Xie, L., Hu, D., Wang, F., & Qu, T. (2006). Observation of Luzon Strait transport. *Geophysical Research Letters*, *33*, L19607. <https://doi.org/10.1029/2006GL026272>
- Wang, D., Liu, Q., Huang, R. X., Du, Y., & Qu, T. (2006). Interannual variability of the South China Sea throughflow inferred from wind data and an ocean data assimilation product. *Geophysical Research Letters*, *33*, L14605. <https://doi.org/10.1029/2006GL026316>
- Wang, G., Huang, R. X., Su, J., & Chen, D. (2012). The effects of thermohaline circulation on wind-driven circulation in the South China Sea. *Journal of Physical Oceanography*, *42*, 2283–2296. <https://doi.org/10.1175/JPO-D-11-0227.1>
- Wang, G., Xie, S. P., Qu, T., & Huang, R. X. (2011). Deep South China Sea circulation. *Geophysical Research Letters*, *38*, L05601. <https://doi.org/10.1029/2010GL046626>
- Wyrtki, K. (1961). Scientific results of marine investigations of the South China Sea and the Gulf of Thailand 1959–1961. NAGA Report 2.
- Xu, F.-H., & Oey, L.-Y. (2014). State analysis using the Local Ensemble Transform Kalman Filter (LETKF) and the three-layer circulation structure of the Luzon Strait and the South China Sea. *Ocean Dynamics*, *64*(6), 905–923. <https://doi.org/10.1007/s10236-014-0720-y>
- Xue, H., Chai, F., Pettigrew, N., Xu, D., Shi, M., & Xu, J. (2004). Kuroshio intrusion and the circulation in the South China Sea. *Journal of Geophysical Research*, *109*, C02017. <https://doi.org/10.1029/2002JC001724>
- Yang, J., & Price, J. F. (2000). Water-mass formation and potential vorticity balance in an abyssal ocean circulation. *Journal of Marine Research*, *58*(5), 789–808. <https://doi.org/10.1357/002224000321358918>
- Yuan, D. (2002). A numerical study of the South China Sea deep circulation and its relation to the Luzon Strait transport. *Acta Oceanologica Sinica*, *21*(2), 187–202.
- Zhu, Y., Sun, J., Wang, Y., Wei, Z., Yang, D., & Qu, T. (2017). Effect of potential vorticity flux on the circulation in the South China Sea. *Journal of Geophysical Research: Oceans*, *122*, 6454–6469. <https://doi.org/10.1002/2016JC012375>